Electronic Transition Oscillator Strengths in Solids: An Extended Hückel Tight-Binding Approach

Ruedi Rytz and Gion Calzaferri*

Department of Chemistry and Biochemistry, University of Berne, Freiestrasse 3, CH-3000 Bern 9, Switzerland

Received: March 12, 1997[⊗]

A method for calculating electronic dipole-induced transitions in solids based on extended Hückel tight-binding (EHTB) wave functions is presented. The proposed computational treatment relies on the position formulation for intensity calculations. It is compared with the well-known velocity method that involves differentiation of the wave functions with respect to the electron positions. The described CEDiT (crystal electronic dipole-induced transitions) computations are applied to interpret the low-energy absorption spectrum of polyacetylene and the group VIA transition metal dichalcogenide MoS_2. Good agreement between calculation and experimental absorption spectra is obtained. In the case of polyacetylene the first prominent absorption band is due to $\pi^* \leftarrow \pi$ transitions about the Z point of the irreducible Brillouin zone. The high density of states (DOS) encountered at Z can be identified as responsible for the characteristic shape of this band. For MoS_2 we plot the oscillator strengths of the first four prominent electronic transitions as a function of the $\mathbf{k}$ vector in the irreducible Brillouin zone. The excitonic transitions A and B are due to resonance of two almost degenerate interband absorptions confined to a relatively well-defined region in $\mathbf{k}$ space at about $\mathbf{k}_A = (^{22}/_{57}, {}^2/_{57})$ and $\mathbf{k}_B = (^1/_3, {}^2/_{57})$, respectively. The origin in $\mathbf{k}$ space of the interband absorptions C and D is also discussed.

1. Introduction

Understanding of the interaction of light with solids is of fundamental interest not only in order to gain insight into the solid's electronic structure but also to help us to design new optical devices. The physics in this area is quite rich, as are the experimental techniques.[1] Hence, it would be a very demanding or even impossible chore to model the optical properties of solids ranging from insulators through semiconductors to metals and treating excitons, interband transitions, and plasmons in a uniform way. Fundamental questions such as "What is the mechanism by which matter absorbs visible or ultraviolet light at a given wavelength? and How does it dispose of the energy it thereby acquires?" have been answered satisfactorily in the case of atoms and simple molecules, but in the case of solids, experimental facts immediately overwhelm any simple quantitative theory. However, an indispensable prerequisite in order to describe light absorption or emission phenomena in solids is the knowledge of its electronic structure. Since the turn of this century when Drude put forth his noted theory,[2,3] many—more or less sophisticated—methods aiming at the description of the electronics of solids have been developed. It has been shown that the band structure in the band-gap region is frequently well describable within the extended Hückel tight-binding (EHTB) theory.[4−6] This usually holds for semiconductors that have been the focus of intense research for their optical properties and their capability to transform visible light to electrical energy in solar devices.[7−12] On the other hand, it is well documented in the literature—starting with the pioneering work of Wolfsberg and Helmholz—that electronic transitions in molecules can be often well treated within the extended Hückel (EHMO) approximation.[13,14] In a recent publication, we successfully applied oscillator strength calculations to describe electronic dipole-induced transitions

(EDiTs) based on EHMO wave functions for computing different types of transitions found in molecules, clusters, and complexes.[15] It has been challenging to investigate if the same electronic dipole formalism can be extended to the solid state as long as initial and final states of the transitions can be associated with EHTB wave functions. We have therefore developed a FORTRAN program which we call CEDiT (crystal electronic dipole-induced transitions) that allows the modeling of electronic absorption spectra of solids based on this approach.

A number of theoretical expressions for the description of electronic dipole transitions have been reported. Their equivalence for exact wave functions can be proven by canonical transformations of the Hamiltonian[16,17] or can be shown to be a consequence of the off-diagonal hypervirial relation for an arbitrary quantum mechanical operator.[18] The two most common versions are the position and the velocity formulation employing the quantum mechanical operators $\mathbf{r}_i$ and $\nabla_{\mathbf{r}_i}$, respectively. For molecules it is known that these two formulations in general do not yield identical oscillator strengths if applied to approximate wave functions.[19,20]

In this work we report applications of CEDiT calculations on polyacetylene and the group VIA transition metal dichalcogenide MoS_2 that has been reinvestigated in a recent publication[10] using the *position* operator for the computation of the transition dipole elements. It will be shown that the *velocity* formulation on general grounds cannot yield satisfactory results if used in conjunction with extended Hückel tight-binding crystal orbitals. Besides attempting a description of the spectral features of the low-energy transitions that are well-known and have been discussed in the literature,[7,9,21,22] we place the question of the nature of the crystal orbitals (COs) engaged and the origin in $\mathbf{k}$ space of these transitions into the foreground, facts that are often difficult to unambiguously determine from experimental data.

This paper is organized as follows: In the next section we describe the computational method as used in this work to model the low-energy electronic spectra of solids. We then proceed

---

* Author to whom correspondence should be addressed.
⊗ Abstract published in *Advance ACS Abstracts,* July 1, 1997.

with a discussion of possible deficiencies of this method. In this connection some general remarks on the oscillator strength calculations in extended systems are made, therewith delimiting the CEDiT procedure from different approaches reported in the literature. The last section is dedicated to applications of CEDiT to polyacetylene and to MoS_2.

2. Method

The Position Formulation. The electronic transition dipole moment $\mathbf{d}_{nm}^{ed}$ between two wave functions ψ_n and ψ_m is defined as[23-25]

$$\mathbf{d}_{nm}^{ed} = \langle \psi_n | \mathbf{d}_{ed} | \psi_m \rangle \qquad (1)$$

$$\mathbf{d}_{ed} = -(\sum_i e\mathbf{r}_i) \qquad (2)$$

The oscillator strength f_{nm} of the transition $n \leftarrow m$ amounts to

$$f_{nm} = \frac{8\pi^2 \tilde{\nu} c m_e}{3he^2} |\mathbf{d}_{nm}^{ed}|^2 \qquad (3)$$

Making use of the definition of the transition dipole length D_{nm}

$$|D_{nm}|^2 := \frac{1}{e^2} |\mathbf{d}_{nm}^{ed}|^2 \qquad (4)$$

we find

$$f_{nm} = l_0 \tilde{\nu} |D_{nm}|^2 \qquad (5)$$

where e is the elementary charge, h is Planck's constant, m_e is the electron mass, c is the speed of light in vacuum, $\mathbf{r}_i$ are the electron position vectors, $\tilde{\nu}$ is the wavenumber in cm^{-1} of the transition $n \leftarrow m$, and l_0 equals 1.085×10^{-5} cm/Å². f_{nm} is dimensionless. Typical f_{nm} values for electronic dipole-allowed transitions are in the range 10^{-3} to 1.

The EHTB band orbitals $\psi_{i\mathbf{k}}(\mathbf{r})$ are given as follows:

$$\psi_{i\mathbf{k}}(\mathbf{r}) = \sum_\mu c_\mu^i(\mathbf{k}) \{ \sum_{\mathbf{R}} e^{i\mathbf{k}\cdot\mathbf{R}} \chi_\mu(\mathbf{r} - \mathbf{R}) \} \qquad (6)$$

where $\mathbf{k}$ is the wave vector and $\chi_\mu(\mathbf{r} - \mathbf{R})$ are the atomic orbitals located at the Bravais lattice sites defined by a set of position vectors

$$\mathbf{R} = n_1\mathbf{a}_1 + n_2\mathbf{a}_2 + n_3\mathbf{a}_3 \qquad (7)$$

in which the n_i run over all integers and the $\mathbf{a}_i$ are linearly independent basic translations. The c_μ^i are the orbital coefficients to be determined by the variation principle. We denote the initial and final crystal orbital (CO) with $\psi_{i\mathbf{k}}$ and $\psi_{f\mathbf{k}'}$, respectively. As we will only consider direct transitions, we may write $\mathbf{k} = \mathbf{k}'$. $f_{fi,\mathbf{k}}$ is then proportional to the energy gap between the two COs at the point $\mathbf{k}$, $\tilde{\nu}(\mathbf{k})$, and to $|D_{fi,\mathbf{k}}|^2$, but the factor l_0 has to be doubled if $\psi_{i\mathbf{k}}$ is occupied by two electrons. Combining eqs 1 and 4 with 6, we find for the transition dipole length

$$D_{fi,\mathbf{k}} = \langle \psi_{f\mathbf{k}} | \mathbf{r} | \psi_{i\mathbf{k}} \rangle$$

$$= \sum_{\mathbf{R},\mu} (c_\mu^f(\mathbf{k}) e^{i\mathbf{k}\cdot\mathbf{R}})^* \sum_{\mathbf{R}',\nu} (c_\nu^i(\mathbf{k}) e^{i\mathbf{k}\cdot\mathbf{R}'}) \times$$

$$\langle \chi_\mu(\mathbf{r} - \mathbf{R}) | \mathbf{r} | \chi_\nu(\mathbf{r} - \mathbf{R}) \rangle \quad (8)$$

Hence, $D_{fi,\mathbf{k}}$ can be written as a matrix containing integrals over atomic orbitals. The summation runs over all atomic orbitals

μ and ν in the unit cells located at $\mathbf{R}$ and $\mathbf{R}'$, respectively. While μ and ν are limited by the size of the unit cell, there is no *per se* restriction for the number of unit cells denoted by $\mathbf{R}$ and $\mathbf{R}'$. Before addressing this point, we make a few general remarks on tight-binding calculations that will help us to solve this problem.

In order to keep the burden of notation minimal, we restrict the following discussion to the simplest possible "solid", namely, a one-dimensional chain of equally spaced hydrogen atoms. Once we have understood the hydrogen chain, the extension to systems of more complicated unit cells and higher dimension should be straightforward.

Any of the N members (points) of the lattice can by definition be described by a vector $\mathbf{R}$ with $\mathbf{R} = n_1\mathbf{a}_1$. If we place a hydrogen atom in every lattice point and assume that $|\mathbf{a}_1| \gg a_0$, where a_0 is the Bohr radius ($a_0 = 0.529 \times 10^{-8}$ cm), then according to basic quantum mechanical considerations, this system can be described by N linear combinations of the respective $1s_H$ orbitals. In order to satisfy the Bloch condition

$$\psi(\mathbf{r} + \mathbf{R}) = e^{i\mathbf{k}\cdot\mathbf{R}}\psi(\mathbf{r}) \qquad (9)$$

appropriate linear combinations are

$$\psi_{i\mathbf{k}} = \sum_{\mathbf{R}} e^{i\mathbf{k}\cdot\mathbf{R}} 1s_H(\mathbf{r} - \mathbf{R}) \qquad (10)$$

where $0 \leq \mathbf{k} \leq 1/2$ ranges through the N values in the first Brillouin zone consistent with the Born–von Kármán periodic boundary condition and $\mathbf{R}$ ranges over all unit cells.[1] Equation 10 corresponds to the part in curly braces in eq 6 that is, the c_μ^i's equal $1/\sqrt{N}$ and there is no $\mathbf{k}$ dependence of the COs. Any H orbital does not "feel" its neighbor and hence does not know of its phase. Therefore all Bloch functions belong to the same energy eigenvalue, namely, -13.6 eV per unit cell (cf. Figure 1a, left). As the Bravais lattice is infinite, there is no way of distinguishing between different sites, and we may choose any point to set up the origin of the coordinate system ($\mathbf{r} = \mathbf{0}$). If we now decrease the lattice constant, the pure hydrogen orbital $1s_H(\mathbf{0})$ begins to experience its neighbors, the $1s_H(\mathbf{0})$, and with it all others, will be more or less perturbed, and the phase of neighboring atoms becomes crucial. The c_μ^i's alter their value as a function of $\mathbf{k}$. At the point $\mathbf{k} = 0$ (Γ point) all orbitals are in-phase and hence only have bonding interaction, and their energy drops to about -20 eV. The opposite holds for a hydrogen in a Bloch function at the X point. Any hydrogen orbital has antibonding interaction with either of its immediate neighbors. Their energy rises to ~30 eV (cf. Figure 1a, right). It is important to stress that $1s_H(\mathbf{0})$ will only be affected by a few nearest neighbors; thus the determination of the c_μ^i's can be restricted to only a few neighbor cells (N_{EHTB}). We will see that the same should hold for the transition dipole length $D_{fi,\mathbf{k}}$.

Let us now address the calculation of the transition dipole length. For simplicity we inspect transitions at the center of the Brillouin zone (i.e. $\mathbf{k} = \mathbf{0}$). Applying the above definitions, $D_{fi,\mathbf{0}}$ can be written as

$$D_{fi,\mathbf{0}} = \sum_{M_1=-N}^{N} \sum_{M_2=-N}^{N} \frac{1}{2N + 1 - |M_1 - M_2|} \times$$

$$\langle \sum_\mu c_\mu^f \chi_\mu(\mathbf{x} - M_1\mathbf{a}_1) | \mathbf{x} | \sum_\nu c_\nu^i \chi_\nu(\mathbf{x} - M_2\mathbf{a}_1) \rangle \quad (11)$$

where the sums run over only a few neighbor cells N relative to the reference cell at $\mathbf{x} = \mathbf{0}$, where the photon is supposed to hit. We have made the assumption that all electrons in the N next neighbor cells experience the same electric force that is ordinarily satisfied as the wavelength λ of visible light is on the order of between 10^3 and 10^4 Å, whereas the lattice constant
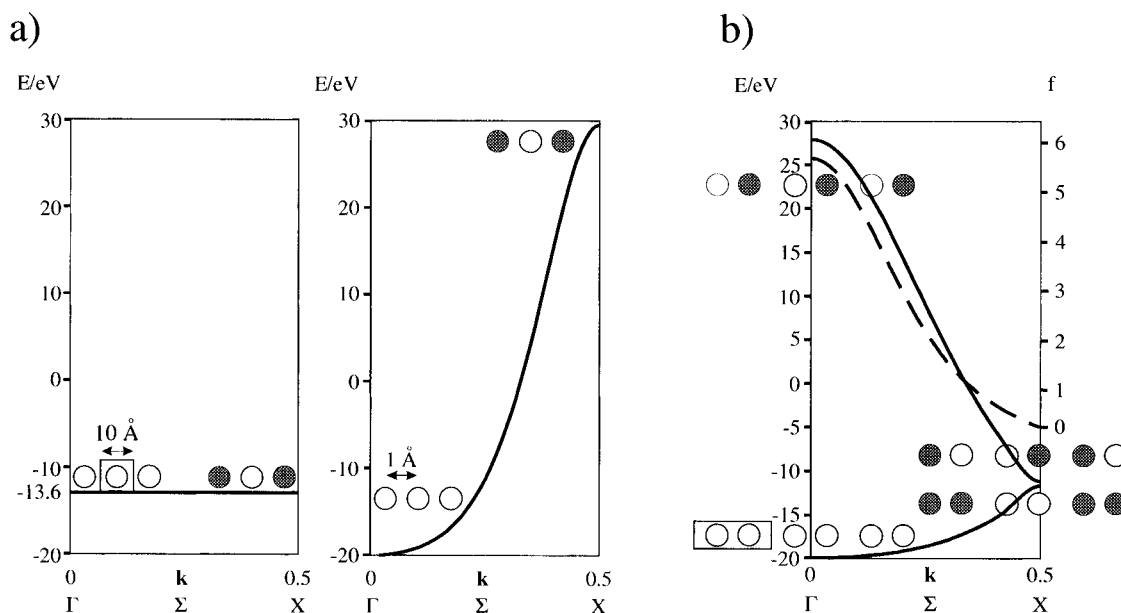
Figure 1. (a) Band structure of a chian of hydrogen atoms spaced 10 and 1 Å apart, respectively. The energy of an isolated H atom is −13.6 eV. (b) Band structure of a Peierls distorted H chain. A distortion of 0.01 Å is assumed. The computed oscillator strength *f* along the Σ line is drawn as a dashed line.

$\mathbf{a}_1$ is usually on the order of angstrøms. The normalization factor $1/(2N + 1 - |M_1 - M_2|)$ is introduced for the following reason: in a tight-binding calculation the determination of the coefficients $c_\mu^i(\mathbf{k})$ must not depend on the number of neighbor cells considered around the cell lying at $\mathbf{R} = 0$. This condition can be easily fulfilled, as the overlap responsible for the distortion of the atomic orbital(s) decreases rapidly with increasing distance of the interacting cells. This, however, does not hold for eq 11 without the mentioned normalization. At $\mathbf{k} = 0$ all coefficients of atomic orbitals related to each other by translation through a multiple of the lattice constant $\mathbf{a}_1$ are the same. Thus, increasing the number of neighbors N would increase the number of equal transition dipole length elements and hence the oscillator strength. The correction is to divide every matrix element by the number of identical ones. Convergence is reached as soon as the elements $\langle c_\mu^f \chi_\mu(x + N\mathbf{a}_1)|\mathbf{x}|c_\nu^i \chi_\nu(x - N\mathbf{a}_1)\rangle$ approach zero. This condition can usually be satisfied by setting the number of neighbor cells for a CEDiT calculation (N_{CEDiT}) to approximately half of the neighbor cells used in the respective band calculation: $N_{\text{CEDiT}} \approx N_{\text{EHTB}}/2$.

We consider again the H chain sketched in Figure 1a. From the point of view of an oscillator strength calculation both situations are equally uninteresting. For any given $\mathbf{k}$ point only one Bloch function exists exhibiting the needed translational symmetry. Direct dipole-allowed transitions with $\mathbf{k}_{\psi i} = \mathbf{k}_{\psi f}$ do not exist.

Chemists would expect such a hydrogen chain to break apart forming H_2 molecules. Such breaking apart would be due to vibronic coupling and is nothing else but the well-known Peierls distortion. This leads to the situation sketched in Figure 1b. The unit cell now contains two hydrogen atoms. For any $\mathbf{k}$ vector we can construct two Bloch functions, resulting in two bands. The lower band runs up as we move from Γ to X; the upper band runs down. They almost meet at X. The only difference between the two crystal orbitals at this point is that the more stable CO exhibits bonding interaction within (shorter distance) and the slightly destabilized one across the unit cell (longer distance). They would be exactly the same if we removed the Peierls distortion, taking us back to the situation sketched in Figure 1a, with the important difference that we have doubled the size of the unit cell. This means twice the

number of basis functions and thus twice the number of bands. However, the energy range covered by the single band in Figure 1a and in the case described above remains the same. This fact is called back-folding.[4] In a Peierls distorted chain we obviously have the possibility of computing direct electronic transitions. The same holds for the "back-folded" hydrogen chain, even though this is in clear contradiction to what we have stated above. As physical properties should not depend on assumptions above the size of the unit cell, we conclude that we have to restrict our calculations to the primitive unit cell. This notion is further supported by the following observation. In a "back-folded" hydrogen chain the two crystal orbitals are degenerate at X. Hence, $D_{fi,X}$ must be equal to zero for symmetry reasons. However, $D_{fi,X} = 1.18$ Å is computed if we take two basis functions to treat an equally spaced chain of H atoms. The energy range—the allowed energies as we move through $\mathbf{k}$ space—is independent of the relative phase of the crystal orbitals; the transition dipole length is not. To obtain the correct answer ($D_{fi,X} = 0$ Å) in a "back-folded" chain of equally spaced hydrogens, we would have to shift any of the respective crystal orbitals by half of the unit cell length. This, however, requires knowledge of the translational symmetry of the crystal orbital, a property that is supposed to be fully taken care of by the Bloch functions alone. Hence, the simplest solid allowing a physically meaningful oscillator strength calculation is a Peierls distorted H chain.

In Figure 1b we give the calculated oscillator strength as a function of the $\mathbf{k}$ vector (dotted line). The highest absorption intensity is found at Γ; the lowest at X, where it is almost zero. This finding is not too surprising for the following reasons. Firstly, the energy difference decreases quite dramatically as we move from Γ to X; secondly, the transition dipole length decreases as initial and final crystal orbitals begin to resemble each other more and more on going from Γ to X (cf. eq 11).

At points of high symmetry in the first Brillouin zone (e.g. Γ point) degenerate crystal orbitals are frequently observed. Thus, a few words about oscillator strengths between degenerate COs will be added. Any electron occupying the degenerate initial crystal orbital may be promoted to any crystal orbital of the degenerate final set. Hence, the formula for the $f_{fi,\mathbf{k}}$ takes the form

$$f_{fi,\mathbf{k}} = 2l_0 \tilde{\nu} \frac{\bar{b}}{2} \frac{\sum_{n=1}^{G_q} \sum_{m=1}^{G_r} f_{nm,\mathbf{k}}}{G_r} \tag{12}$$

where G_r and G_q indicate the degeneracy of the initial and the final COs, respectively. The averaged occupation number of the initial CO is denoted by $\bar{b}$; the 2 in the denominator takes into consideration that the factor $2l_0$ is calculated for occupied orbitals. $\bar{b}$ can be easily determined in diamagnetic solids by filling up all valence bands. The same procedure turns out to be much more cumbersome in paramagnets involving numerical integration up to the Fermi energy ϵ_f.

Up to now we have only considered electronic dipole-induced transitions at distinct $\mathbf{k}$ points. However, transitions contributing to the electronic absorption spectrum of a solid may occur at any $\mathbf{k}$ point within the irreducible Brillouin zone (IBZ), and we will see that it is of great importance to take all these points into account. It is not sufficient to restrict the calculation to points or lines of high symmetry of the IBZ. High densities of state (DOS) given by

$$g(\epsilon) = \left(\frac{d\epsilon(\mathbf{k})}{dn}\right)^{-1} \tag{13}$$

where n is the number of one-electron levels in the energy range $\epsilon + d\epsilon$, often encountered at these "special" points in general do not guarantee high electronic absorption; low oscillator strengths may destroy this notion. For the two-dimensional IBZ we apply a numerical integration procedure as described by Ramírez and Böhm.[26] The integral I of a periodic function $p(\mathbf{k})$ (e.g. oscillator strength $f_{fi}(\mathbf{k})$) can be approximated by a discrete summation

$$I = \frac{1}{V_{IBZ}} \int_{IBZ} p(\mathbf{k}) \, d\mathbf{k} \approx \frac{1}{N} \sum_i \omega_i p_i(\mathbf{k}) \tag{14}$$

where ω_i is the weight of the ith data point as determined by simple geometrical reasoning, and N normalizes the weighting factors to unity: $N = \sum_i \omega_i$.

Other Formalisms for Intensity Calculations. In the previous section we have introduced the theory as implemented in the CEDiT program and used to model the low-energy absorption spectra of polyacetylene and MoS_2 (vide infra). We proceed by discussing the oscillator strength calculations in extended systems in a more general way in order to deliminate our procedure from different approaches reported in the literature.

Theoretical expressions for electronic intensities are available in a number of equivalent forms.[16,17,27] The two most common versions are the following electronic dipole relations

$$\langle \psi_n | \sum_i \nabla_{\mathbf{r}_i} | \psi_m \rangle = \langle \psi_n | [\sum_i \mathbf{r}_i, \mathcal{H}] | \psi_m \rangle = \omega_{nm} \langle \psi_n | \sum_i \mathbf{r}_i | \psi_m \rangle \tag{15}$$

$$\langle \psi_n | \sum_i (\nabla_{\mathbf{r}_i} V) | \psi_m \rangle = \langle \psi_n | [\sum_i \nabla_{\mathbf{r}_i}, \mathcal{H}] | \psi_m \rangle = \omega_{nm} \langle \psi_n | \sum_i \nabla_{\mathbf{r}_i} | \psi_m \rangle \tag{16}$$

where we have used atomic units; that is, $\hbar = m_e = e = 4\pi\epsilon_0 = 1$, m_e and e being the mass and the charge of an electron, respectively. Here $\mathbf{r}_i$ and $\nabla_{\mathbf{r}_i}$ are the position and the gradient vectors for the ith electron, and V is the local potential energy. For molecules it has been shown that the position (eq 15) and

the velocity (eq 16) formulation yield identical results only under the condition that exact wave functions and transition energies are used in the computations. Most approximate calculations exhibit discrepancies among the results obtained from these expressions.[19,20] The same holds for band calculations where the situation is further complicated by the introduction of the translational symmetry and therewith fundamentally changing the behavior of quantum mechanical operators.

We consider one-electron interband transitions between fully occupied and empty bands. It can be shown that orbitals not changing their occupation under irradiation do not contribute to the oscillator strength.[24] Hence, we may drop the sums in eqs 15 and 16 and write $\mathbf{r}$ and $\nabla_{\mathbf{r}}$ for the position and velocity operators, respectively. We first check whether these operators if applied to Bloch *sums* (cf. eq 6) are hermitian. The hermiticity (i.e. $\langle n | \mathcal{O} m \rangle = \langle m | \mathcal{O} n \rangle^*$) of the position operator $\mathbf{r}$ can be demonstrated as follows:[28]

$$\langle \psi_{n\mathbf{k}} | \mathbf{r} | \psi_{m\mathbf{k}} \rangle = \int_{-\infty}^{\infty} \psi_{n\mathbf{k}}^*(\mathbf{r}) \, \mathbf{r} \, \psi_{m\mathbf{k}}(\mathbf{r}) \, d\mathbf{r} =$$

$$\int_{-\infty}^{\infty} \psi_{m\mathbf{k}}(\mathbf{r}) \, \mathbf{r} \, \psi_{n\mathbf{k}}^*(\mathbf{r}) \, d\mathbf{r}$$

$$= \{\int_{-\infty}^{\infty} \psi_{m\mathbf{k}}^*(\mathbf{r}) \, \mathbf{r} \, \psi_{n\mathbf{k}}(\mathbf{r}) \, d\mathbf{r}\}^* = \langle \psi_{m\mathbf{k}} | \mathbf{r} | \psi_{n\mathbf{k}} \rangle^* \tag{17}$$

with $(\psi^*)^* = \psi$ and $\mathbf{r}$ is real. It is already implicit in eq 15 and only a bit obscured by the notation that the velocity−dipole relation

$$\mathbf{p}_{nm,\mathbf{k}} = -\frac{im_e\omega_{nm,\mathbf{k}}}{e} \mathbf{d}_{nm,\mathbf{k}}^{ed} \tag{18}$$

makes use of the momentum operator $\mathbf{p} = (\hbar/i)\nabla_{\mathbf{r}}$ rather than $\nabla_{\mathbf{r}}$.[28] Applying integration by parts, we thus write

$$\langle \psi_{n\mathbf{k}} | \mathbf{p} | \psi_{m\mathbf{k}} \rangle = \int_{-\infty}^{\infty} \psi_{n\mathbf{k}}^*(\mathbf{r}) \frac{\hbar}{i} \nabla_{\mathbf{r}} \psi_{m\mathbf{k}}(\mathbf{r}) \, d\mathbf{r}$$

$$= \frac{\hbar}{i} \int_{-\infty}^{\infty} \psi_{n\mathbf{k}}^*(\mathbf{r}) \, d\psi_{m\mathbf{k}}(\mathbf{r})$$

$$= \frac{\hbar}{i} \{\psi_{n\mathbf{k}}^*(\mathbf{r}) \, \psi_{m\mathbf{k}}(\mathbf{r}) - \int \psi_{m\mathbf{k}}(\mathbf{r}) \, d\psi_{n\mathbf{k}}^*(\mathbf{r})\}|_{\mathbf{r}=-\infty}^{\mathbf{r}=+\infty}$$

$$= \psi_{n\mathbf{k}}^*(\mathbf{r}) \, \psi_{m\mathbf{k}}(\mathbf{r})|_{\mathbf{r}=-\infty}^{\mathbf{r}=+\infty} - \int_{-\infty}^{\infty} \psi_{m\mathbf{k}}(\mathbf{r}) \frac{\hbar}{i} \nabla_{\mathbf{r}} \psi_{n\mathbf{k}}^*(\mathbf{r}) \, d\mathbf{r}$$

In order to obtain hermiticity the first term is required to vanish, which is generally the case for "molecular" wave functions that approach zero at $\mathbf{r} \pm \infty$. Bloch *sums*, however, by construction neither vanish at $\mathbf{r} \pm \infty$ nor are they periodic in the direct Bravais lattice (i.e. $\psi_{n\mathbf{k}}(\mathbf{r}) \neq \psi_{n\mathbf{k}}(\mathbf{r} + \mathbf{R})$). The functional values of Bloch *sums* at infinity, i.e. $\psi_{n\mathbf{k}}(\infty)$ or $\psi_{n\mathbf{k}}(-\infty)$, are defined mathematically. This does not hold, however, for the limits $\pm\infty$ themselves, as infinity in a Bravais lattice is "everywhere". $\mathbf{r} \pm \infty$ are neither distinguished nor well-defined places in the lattice. It should be noted that there is nothing in the Born−von Kármán periodic boundry condition that defines the value of the Bloch *sums* at $\mathbf{r} \pm \infty$; in particular they are not forced to be equal. The periodic boundry condition merely allows us to equate the number of Bloch wave vectors $\mathbf{k}$ in a primitive cell of the reciprocal lattice. Thus, the infinity of the Bravais lattice is taken into account by a vector $\mathbf{k}$ that becomes continuous throughout the first Brillouin zone as $\mathbf{R} \rightarrow \infty$.

TABLE 1: Real and Imaginary Part of the Dipole Length Times e^2 (i.e. d_{nm}^{ed}) Calculated in Absorption $\psi_{2k} \leftarrow \psi_{1k}$ and Emission $\psi_{1k} \leftarrow \psi_{2k}$, Numerically Showing the Hermiticity of the Operator x (or r) As Applied to Bloch *Sums*

k point	Re[$\mathbf{d}_{12}$]	Im[$\mathbf{d}_{12}$]	Re[$\mathbf{d}_{21}$]	Im[$\mathbf{d}_{21}$]
0.0	−1.562 306 87	0.0	−1.562 306 87	0.0
0.1	−1.491 663 06	0.001 335 161 2	−1.491 663 06	−0.001 335 161 2
0.2	−1.320 137 70	0.002 041 021 3	−1.320 136 70	−0.002 041 021 3
0.3	−1.131 277 76	0.002 586 304 6	−1.131 277 76	−0.002 586 304 6
0.4	−0.994 007 05	0.002 659 343 6	−0.994 007 05	−0.002 659 343 6
0.5	−0.944 940 15	4.3298×10^{-11}	−0.944 940 15	-4.3298×10^{-11}

For completeness, we finish the proof under the condition that the first term vanishes.

$$\langle\psi_{nk}|\mathbf{p}|\psi_{mk}\rangle = -\frac{\hbar}{i}\int_{-\infty}^{\infty}\psi_{mk}(\mathbf{r})\,d\psi_{nk}^{*}(\mathbf{r})$$

$$= \left\{\int_{-\infty}^{\infty}\psi_{mk}^{*}(\mathbf{r})\frac{\hbar}{i}\nabla_{\mathbf{r}}\psi_{nk}(\mathbf{r})\,d\mathbf{r}\right\}^{*} =$$
$$\langle\psi_{mk}|\mathbf{p}|\psi_{nk}\rangle^{*}\quad(19)$$

Hence, the momentum operator $\mathbf{p}$ is not hermitian if applied to Bloch *sums*. As the oscillator strength f_{nm} is an observable and proportional to $|\mathbf{d}_{nm}^{ed}|^2 = \mathbf{d}_{nm}^{ed}\mathbf{d}_{mn}^{ed}$ (cf. eq 3), the matrix elements $\mathbf{d}_{nm}^{ed}$ are required to be hermitian. In Table 1 we list $\mathbf{d}_{12}(\mathbf{k})$ and $\mathbf{d}_{21}(\mathbf{k})$ taken from our oscillator strength calculation on the Peierls distorted H chain shown in Figure 1b, therewith numerically showing the hermiticity of the operator $\mathbf{r}$.

This does not mean that $\mathbf{p} = (\hbar/i)\nabla_{\mathbf{r}}$ is not an admissible operator. It only demonstrates that it is not hermitian, if we apply it to Bloch *sums*. It is, however, always possible to construct well-localized wave packets out of Bloch *sums*, thereby fulfilling the condition of vanishing wave functions when $\mathbf{r}$ is infinite. Another possibility that will be considered toward the end of this section is the transformation of Bloch *sums* to Bloch *functions*. Bloch *functions* are periodic in the direct Bravais lattice, which turns $\mathbf{p}$ into a hermitian operator. If $\mathbf{p}$ is applied to Bloch *sums*, some care is, however, advisable, as can easily be demonstrated for the Peierls distorted H chain. The crystal orbitals at the Γ point are given by

$$\psi_{1,0}(\mathbf{r}) = N_1^{-1/2}\sum_{\mathbf{R}}\{1s_{H_1}(\mathbf{r}-\mathbf{R}) + 1s_{H_2}(\mathbf{r}-\mathbf{R})\}$$

$$\psi_{2,0}(\mathbf{r}) = N_2^{-1/2}\sum_{\mathbf{R}}\{1s_{H_1}(\mathbf{r}-\mathbf{R}) - 1s_{H_2}(\mathbf{r}-\mathbf{R})\}\quad(20)$$

where $\psi_{1,0}(\mathbf{r})$ and $\psi_{2,0}(\mathbf{r})$ are the valence and conduction band, respectively. Operating with $\mathbf{p} = (\hbar/i)\nabla_{\mathbf{r}}$ on $\psi_{1,0}$ and expanding the Bloch *sums* in sums of Slater-type orbitals (STOs) of the form $1s_{H_1} = 1s_{H_2} = N_{\zeta}e^{-\zeta\mathbf{r}}$ yields

$$(\hbar/i)\nabla_{\mathbf{r}}\psi_{1,0}(\mathbf{r}) = (\hbar/i)\nabla_{\mathbf{r}}N_1^{-1/2}\sum_{\mathbf{R}}\{1s_{H_1}(\mathbf{r}-\mathbf{R}) +$$
$$1s_{H_2}(\mathbf{r}-R)\}$$

$$= (\hbar/i)N_1^{-1/2}\sum_{\mathbf{R}}\{\nabla_{\mathbf{r}}1s_{H_1}(\mathbf{r}-\mathbf{R}) +$$
$$\nabla_{\mathbf{r}}1s_{H_2}(\mathbf{r}-\mathbf{R})\}$$

$$= -(\hbar/i)\zeta N_1^{-1/2}\sum_{\mathbf{R}}\{1s_{H_1}(\mathbf{r}-\mathbf{R}) +$$
$$1s_{H_2}(\mathbf{r}-\mathbf{R})\}$$

$$= -(\hbar/i)\zeta\psi_{1,0}\quad(21)$$

Hence, the oscillator strength that is proportional to the square of

$$(\hbar/i)\int\psi_{2,0}(\mathbf{r})\,\nabla_{\mathbf{r}}\psi_{1,0}(\mathbf{r})\,d\mathbf{r}\quad(22)$$

is zero according to

$$(\hbar/i)\int\psi_{2,0}(\mathbf{r})\,\nabla_{\mathbf{r}}\psi_{1,0}(\mathbf{r})\,d\mathbf{r} = i\hbar\zeta\int\psi_{2,0}(\mathbf{r})\,\psi_{1,0}(\mathbf{r})\,d\mathbf{r} =$$
$$i\hbar\zeta\delta_{12} = 0\quad(23)$$

It is easy to show that the same holds for any $\mathbf{k} \in$ IBZ. This is an unexpected result and in contrast to the finding of the position representation (cf. Figure 1b). It is difficult to see why electronic interband transitions should be forbidden in a Peierls distorted H chain, whereas it is known that such transitions are responsible for the relatively intense low-energy $\pi^* \leftarrow \pi$ absorption band in the topologically similar polyacetylene.[21]

Another point deserving our attention is the choice of the unit cell. In the previous section, we have given some rather intuitive arguments of why we should restrict the calculation to the smallest (i.e. primitive) unit cell. In this place, we further justify this statement and address the case where an appropriate definition of the unit cell is not straightforward. The starting point is once again the Peierls distorted H chain sketched in Figure 1b. As described above, computation of the crystal orbitals emerging from a chain of equally spaced hydrogen atoms has to be carried out by considering exactly one hydrogen atom per unit cell such that the translational symmetry is fully taken into account by the phase factor $e^{i\mathbf{k}\cdot\mathbf{R}}$. We have already mentioned that the energy gap appearing at the X point in Figure 1b would close upon destruction of the Peierls distortion, therewith enforcing the hydrogens to be equally spaced. It is furthermore not difficult to see that the energy range covered by the unfolded chain (right-hand side of Figure 1a) and the back-folded band are equal and limited by the all-bonding and all-antibonding crystal orbitals. This is, however, the only property these two "pictures" have in common! Computing the bands with two H atoms per unit cell and starting with the most bonding crystal orbital at Γ, the band runs from Γ to X and then back to Γ until the maximum energy is reached. This does not hold for the "not-back-folded" situation, where the whole energy range is already scanned upon going from Γ to X. Hence, it is clear that the slope of the band (i.e., $\partial\epsilon(\mathbf{k})/\partial\mathbf{k}$) is different in both cases. As various physical properties are connected with the slope of the bands, this has far-reaching consequences such as different Fermi levels, crystal energies, electron velocities, and oscillator strengths. *Thus a smallest or primitive unit cell, as it is often called, always has to be considered.* The conception of back-folding is, however, a very useful didactical tool and helpful to treat small distortions of the crystal that enlarge the unit cell.[4] There is no unique way of choosing a primitive cell for a given Bravais lattice. We restrict the discussion to the Wigner−Seitz cell without losing generality. Since there is nothing in the definition of the Wigner−Seitz cell that refers to any particular choice of
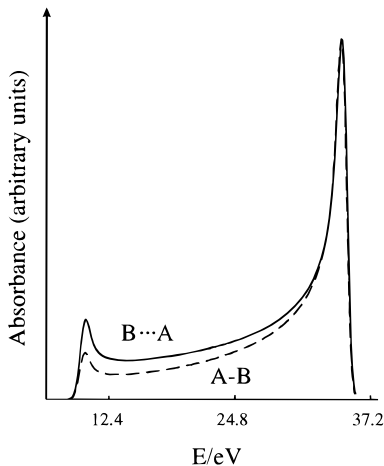
Figure 2. Computed spectra of a linear A−B chain. The distances between A−B and B···A are chosen to be 1.0 and 1.5 Å, respectively. The dashed and solid line show the spectra for a A−B and B···A unit cell, respectively, normalized to the main absorption band.

primitive vectors, the Wigner−Seitz cell will be as symmetrical as the Bravais lattice.[1]

A physical crystal can be described by giving its underlying Bravais lattice, together with a description of the arrangement of atoms, molecules, ions, etc., within a particular primitive cell (i.e. by defining a basis with respect to the Bravais lattice points). The choice of such a basis within a Wigner−Seitz primitive cell is not necessarily unique, even though often given by the chemists intuition of bonding in extended structures, probably placing the most tightly bound species into a unit cell. We consider a one-dimensional chain ···A−B···A−B···A−B··· that consists of two different atoms A and B. Obviously, there are two ways in which the basis regarding the one-dimensional Bravais lattice can be defined, namely, (a) A−B and (b) B···A. Here, both possibilities fulfill the requirement of being a smallest unit cell. As far as the energy calculation is concerned, the situations a and b will yield equal values, as we would expect it to. In the case of the crystal orbitals, things are already a bit more subtle, as they are no longer the same but shifted by some arbitrary phase factor. However, the hermitian operator **r** is defined with respect to the chosen unit cell. It is not too surprising that the oscillator strength calculation based on Bloch *sums* is to some extent dependent on this choice. To a certain degree this problem can be circumvented by transforming the Bloch *sums* $\psi_{n\mathbf{k}}(\mathbf{r})$ to Bloch *functions* $\varphi_{n\mathbf{k}}(\mathbf{r})$. We will address this point toward the end of this section. For the moment, we argue that photons do not discriminate between different unit cell choices and suggest taking the average value of the computations a and b. The disadvantage of this unit cell dependence is less severe than might be guessed at first glance due to the fact that the oscillator strength is proportional to the square of the transition dipole length. Even, if the transition dipole lengths for different unit cell choices should have opposite signs, only minor changes regarding the computed spectrum are observed. In Figure 2 we show the worked out spectra of a linear A−B chain. The distances between A−B and B···A are chosen to be 1 and 1.5 Å, respectively, resulting in a unit cell size of 2.5 Å. The Slater orbitals and Coulomb integrals are given in Table 2. The dashed and solid lines show the spectra for an A−B and B···A unit cell, respectively, normalized to the main absorption band. This clearly demonstrates that no new features arise upon a different unit cell choice, despite the large overlaps and energies involved in this example. For bigger unit cells and more realistic transition energies these discrepancies are further diminished. We add that once a basis with respect to the Bravais lattice is chosen, the computation

TABLE 2: Coulomb Integrals H_{ii} and Slater Exponents ζ_i

element	orbital	ζ_i (c_i)	H_{ii}/eV
A	1s	1.3	−13.6
B	1s	1.0	−10.0
H	1s	1.3	−13.6
C	2s	1.71	−21.4
	2p	1.625	−11.4
Mo	5s	1.96^a	−8.94
	5p	1.90^a	−5.60
	$4d_1$	$3.814\ (0.512)^b$	−10.43
	$4d_2$	$1.864\ (0.641)^b$	
S	3s	2.283^c	−19.85
	3p	1.817^c	−10.93

^{a} Reference 63. ^{b} Reference 64. ^{c} Reference 65.

of the spectrum no longer allows any ambiguities and is independent of the particular choice of the coordinate system within the unit cell. The computations are moreover invariant regarding the number of unit cells that are taken into account (cf. eq 11).

The unit cell dependence of the integrals

$$I_{n\mathbf{k}',m\mathbf{k}} = \int \varphi_{n\mathbf{k}'}^{*}(\mathbf{r})\,\mathbf{r}\,\varphi_{m\mathbf{k}}(\mathbf{r})\,d\mathbf{r} \qquad (24)$$

where the $\varphi_{m\mathbf{k}}$ are Bloch *functions* of the form

$$\varphi_{n\mathbf{k}}(\mathbf{r}) = e^{i\mathbf{k}\cdot\mathbf{r}}u_{n\mathbf{k}}(\mathbf{r}) \qquad (25)$$

is known in the literature. The following suggestion to rewrite $I_{n\mathbf{k}',m\mathbf{k}}$ was put forward:[29,30]

$$\int \varphi_{n\mathbf{k}'}^{*}\,\mathbf{r}\,\varphi_{m\mathbf{k}}\,d\mathbf{r} = -i\frac{\partial}{\partial\mathbf{k}}\int \varphi_{n\mathbf{k}'}^{*}\varphi_{m\mathbf{k}}\,d\mathbf{r} +$$
$$\int u_{n\mathbf{k}'}^{*}\,e^{[i(\mathbf{k}-\mathbf{k}')\cdot\mathbf{r}]}\frac{i\partial u_{m\mathbf{k}}}{\partial\mathbf{k}}\,d\mathbf{r}$$
$$= -i\frac{\partial}{\partial\mathbf{k}}\int \varphi_{n\mathbf{k}'}^{*}\varphi_{m\mathbf{k}}\,d\mathbf{r} + i\,\Omega_{nm}\,\delta(\mathbf{k}-\mathbf{k}') \qquad (26)$$

The physical notion in eq 26 is the observation that $-i\partial/\partial\mathbf{k}$ is another position operator as can be seen if applied to plane waves.

$$\langle\mathbf{r}\rangle = \delta(\mathbf{k}-\mathbf{k}')\int e^{-i\mathbf{k}'\cdot\mathbf{r}}\,(\mathbf{r})(-i\nabla_{\mathbf{k}})e^{i\mathbf{k}\cdot\mathbf{r}}(\mathbf{r})\,d\mathbf{r} \qquad (27)$$

As Bloch *functions* are in general eigenfunctions neither of the momentum operator nor of the position operator, we get an additional term Ω_{nm} that is not sensitive to the choice of the unit cell, whereas the first term is still subject to such a dependence. Hence, it is clear on general grounds that the above transformation is only somewhat more acceptable than eq 24 and does not remove the overall unit cell sensitivity. By coincidence, the quantities Ω_{nm} are used in the perturbative approach by Genkin and Mednis to describe the frequency-dependent linear electric susceptibility.[31] Some authors use $|\Omega_{nm}(\mathbf{k})|$ as a measure of the oscillator strength simply neglecting the first term in eq 26.[32] The motive for this proceeding is, however, obscure as long as the first term does not vanish.

For Bloch *sums* the periodic functions $u_{n\mathbf{k}}(\mathbf{r}) = u_{n\mathbf{k}}(\mathbf{r}+\mathbf{R})$ are given by the transformation

$$u_{n\mathbf{k}}(\mathbf{r}) = e^{-i\mathbf{k}\cdot\mathbf{r}}\psi_{n\mathbf{k}}(\mathbf{r}) \qquad (28)$$

where $\psi_{n\mathbf{k}}(\mathbf{r})$ is defined according to eq 6. For fixed **r**, $u_{n\mathbf{k}}(\mathbf{r})$ is then defined as a sum over all Bravais lattice points **R**, i.e.

$$u_{n\mathbf{k}}(\mathbf{r}) = \sum_{\mathbf{R}} e^{i\mathbf{k}\cdot(\mathbf{R}-\mathbf{r})}\sum_{\mu} c_{\mu}^{n}(\mathbf{k})\,\chi_{\mu}\,(\mathbf{r}-\mathbf{R}) \qquad (29)$$

where $u_{n\mathbf{k}}(\mathbf{r})$ is indeed periodic in the Bravais lattice, according to

$$u_{n\mathbf{k}}(\mathbf{r} + \mathbf{R}') = \sum_{\mathbf{R}} e^{i\mathbf{k}\cdot(\mathbf{R}-\mathbf{r}-\mathbf{R}')} \sum_{\mu} c_{\mu}^{n}(\mathbf{k}) \, \chi_{\mu}(\mathbf{r} - \mathbf{R}) \quad (30)$$

The equivalence of $u_{n\mathbf{k}}(\mathbf{r})$ and $u_{n\mathbf{k}}(\mathbf{r} + \mathbf{R}')$ follows immediately as the sum in eqs 29 and 30 runs over all Bravais lattice sites. Making use of the transformation from Bloch *sums* to Bloch *functions* would then allow us to write[33]

$$(\varphi_{n\mathbf{k}}(\mathbf{r})|\nabla_{\mathbf{r}}|\varphi_{m\mathbf{k}}(\mathbf{r})\rangle = \int_{\text{cell}} u_{n\mathbf{k}}^{*}(\mathbf{r}) e^{-i\mathbf{k}\cdot\mathbf{r}} \, \nabla_{\mathbf{r}} \, u_{m\mathbf{k}}(\mathbf{r}) e^{i\mathbf{k}\cdot\mathbf{r}} \, d\mathbf{r}$$

$$= \int_{\text{cell}} u_{n\mathbf{k}}^{*}(\mathbf{r}) \, \nabla_{\mathbf{r}} \, u_{m\mathbf{k}}(\mathbf{r}) \, d\mathbf{r} +$$

$$i\mathbf{k} \int_{\text{cell}} u_{n\mathbf{k}}^{*}(\mathbf{r}) \, u_{m\mathbf{k}}(\mathbf{r}) \, d\mathbf{r}$$

$$\equiv M_{nm} + i\mathbf{k}\bar{M}_{nm} \quad (31)$$

for the transition matrix elements in the velocity representation. For electronic dipole-allowed transitions the second term in eq 31 is small compared to M_{nm} and can be neglected. It would be exactly zero for direct transitions where the $\mathbf{k}$ vector doesn't change upon absorption of a photon (orthogonality of Bloch functions with same $\mathbf{k}$ and different band indices). M_{nm} is an integral over a primitive unit cell in direct space. Moreover, the operator $(\hbar/i)\nabla_{\mathbf{r}}$ is hermitian for all continuous functions $u_{n\mathbf{k}}(\mathbf{r})$ with continuous derivatives.[34]

$$\int_{\text{cell}} u_{n\mathbf{k}}^{*}(\mathbf{r}) \frac{\hbar}{i}\nabla_{\mathbf{r}} u_{m\mathbf{k}}(\mathbf{r}) \, d\mathbf{r} - \int_{\text{cell}} \left(\frac{\hbar}{i} \nabla_{\mathbf{r}}\right)^{*} u_{n\mathbf{k}}^{*}(\mathbf{r}) \, u_{m\mathbf{k}}(\mathbf{r}) \, d\mathbf{r} = 0 \quad (32)$$

Equation 32 reduces to

$$\frac{\hbar}{i} \int_{\text{cell}} \{u_{n\mathbf{k}}^{*}(\mathbf{r})(\nabla_{\mathbf{r}} u_{m\mathbf{k}}(\mathbf{r})) + (\nabla_{\mathbf{r}} u_{n\mathbf{k}}^{*}(\mathbf{r}))u_{m\mathbf{k}}(\mathbf{r})\} \, d\mathbf{r} =$$

$$\frac{\hbar}{i} \int_{\text{cell}} \nabla_{\mathbf{r}}(u_{n\mathbf{k}}^{*}(\mathbf{r}) \, u_{m\mathbf{k}}(\mathbf{r})) \, d\mathbf{r} \quad (33)$$

This expression is identical with the surface integral

$$\frac{\hbar}{i} \int_{s} \hat{\mathbf{n}}(u_{n\mathbf{k}}^{*}(\mathbf{r}) \, u_{m\mathbf{k}}(\mathbf{r})) \, d\sigma \quad (34)$$

where $\hat{\mathbf{n}}$ is a unit vector in the direction of the outward normal. It has opposite sign at two opposite points, and therefore the integral vanishes, which proves eq 32. The same result is obtained if we follow the arguments used to derive eq 19. As the functions $u_{n\mathbf{k}}(\mathbf{r})$ are periodic in the Bravais lattice, the value of the integral $\int_{\text{cell}} u_{n\mathbf{k}}^{*}(\mathbf{r})(\hbar/i)\nabla_{\mathbf{r}} u_{m\mathbf{k}}(\mathbf{r}) \, d\mathbf{r}$ remains unchanged upon shifting the integration interval by $\Delta\mathbf{r}$. It is, however, always possible to choose $\Delta\mathbf{r}$ such that either $u_{n\mathbf{k}}(\mathbf{r})$ or $u_{m\mathbf{k}}(\mathbf{r})$ is zero on the surface of the unit cell, thus causing the product $u_{n\mathbf{k}}(\mathbf{r}) \, u_{m\mathbf{k}}(\mathbf{r})$ to vanish.

Equations 28−31 demonstrate a way to work out the oscillator strengths starting with Bloch *sums* in a less unit-cell sensitive fashion. This can only be achieved under the condition of transforming the Bloch *sums* to Bloch *functions* and subsequently applying the velocity formulation for the transition matrix elements. It should be noted, however, that the transformation given by eq 29 is still subject to an indeterminacy. We have already mentioned that the phases of the coefficients $c_{\mu}^{n}(\mathbf{k})$ are sensitive to the unit-cell choice. Thus, the $u_{n\mathbf{k}}(\mathbf{r})$ as calculated from the respective Bloch *sums* will reflect this phase dependence. In addition, we mention that even though Bloch *sums* and Bloch *functions* are closely related (cf. eqs 29−30), they are not equal on general considerations. Bloch *functions* are constructed by multiplying a periodic function in

the Bravais lattice by a factor $e^{i\mathbf{k}\cdot\mathbf{r}}$ at every point. Again we take the linear H chain as an example and consider the all-bonding linear combination as observed at the Γ point, which is obviously periodic in the Bravais lattice. If we multiply this crystal orbital with $e^{i\mathbf{k}\cdot\mathbf{r}}$ at every point $\mathbf{r}$ according to the construction recipe for Bloch *functions*, the hydrogen orbitals that spread over a certain distance, say $\Delta\mathbf{r}$ along the chain, may lose their spherical symmetry, as the values $e^{i\mathbf{k}\cdot\mathbf{r}}$ are not constant over the range of $\Delta\mathbf{r}$. For Bloch *sums* such a situation where the atomic orbitals are "unbalanced" may never be encountered.[35]

It would be desirable to further investigate and compare the different formalisms for computing electronic dipole transitions in extended structures. Here we want to explore the applicability of the position formulation to Bloch *sums* putting up with the deficiency of the unit-cell sensitivity that should, however, not be too severe a problem as discussed above.

Computational Section. The calculation of the matrix elements (cf. eq 8) is cumbersome. The procedure used is the same as described in refs 15 and 24, where the calculation of the transition dipole length reduces to computations of overlap integrals with modified Slater exponents ζ to which the right transformation properties are applied. We use the overlap subroutine as originally implemented in ICON8[36] to calculate the overlap integrals. For further reference see the description of the ICON-EDiT package that performs extended Hückel and oscillator strength calculations on molecules.[37] Our computer program, which we name CEDiT, has been restricted to FORTRAN 77 standards, which makes it easily transferable to most platforms. The crystal orbitals used by CEDiT are computed with a modified[10,38] version of the EHMACC program package.[39]

The EHTB crystal orbital calculations on polyacetylene and MoS_2 are described in refs 10 and 38, respectively. We give the respective valence electron ionization energies (VOIEs) and Slater orbitals in Table 2.

3. Applications

We now apply the computational method outlined above to investigate the low-energy absorption spectra of the one-dimensional polyacetylene and the two-dimensional molybdenum(IV) sulfide. Both materials show a highly anisotropic optical behavior and have recently attracted notable interest. It has been shown that many of their properties can be well described by the EHTB method.[10,38,40]

Polyacetylene. As the simplest member of the class of conducting polymers, (all-*trans*)-polyacetylene (PA) has attracted multidisciplinary interest and extensive research activity since the early 1970s,[41] when a new and more easily accessible synthesis for PA was found.[42,43] Moreover, PA is of significant historical importance for quantum chemistry since the early LCAO-MO studies of linear polyenes by Lennard-Jones[44] and Coulson.[45] Doped PA exhibits the largest electrical conductivity observed in any conducting polymer, with values reported in excess of 10^5 S/cm,[46] and exhibits interesting optical properties.[21]

It is now widely accepted that PA forms a Peierls distorted ground state. Theoretical reasoning by Longuet-Higgins and Salem,[47] X-ray scattering data,[48,49] nutation NMR spectroscopy,[50] and ab initio calculations[51,52] do support bond alternation. Recently, it has been shown that EHTB calculations in its ASED (atom superposition and electron delocalization) form yield alternating C−C bond lengths at the optimized geometry.[38] The band structure is shown in Figure 3. The coordinate system is set up such that the chain runs parallel to the $\mathbf{z}$ axis. The π crystal orbitals (COs) are thus formed by the p_x orbitals located

Electronic Transition Oscillator Strengths in Solids

J. Phys. Chem. B, Vol. 101, No. 29, 1997 **5671**
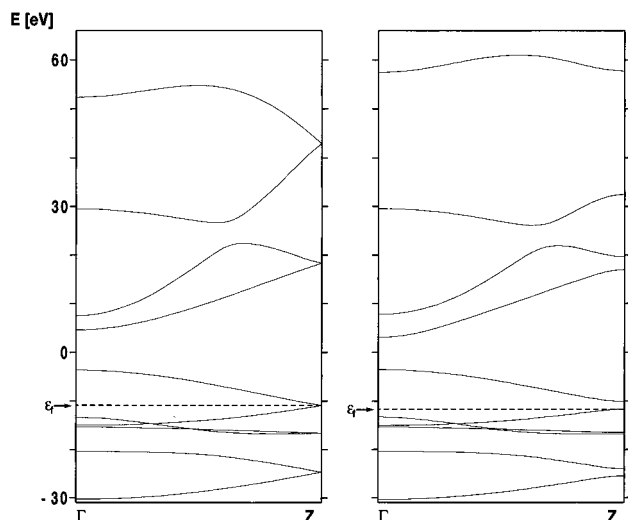

Figure 3. Band structure of (all-*trans*)-polyacetylene with bond alternation (right: C=C 1.36 Å) as compared to the one for equal C−C bond lengths (left: C−C 1.43 Å).
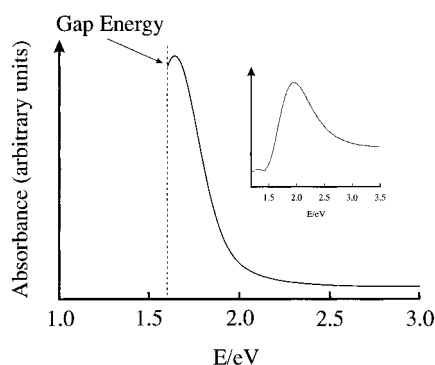

Figure 4. Calculated absorption spectrum of the first $\pi^* \leftarrow \pi$ absorption band of (*all*-trans)-polyacetylene with bond alternation. Only transitions with the light vector parallel to the chain axis are considered. In the inset the transmission spectrum of a spin cast film of *trans*-polyacetylene with poly(vinylbutyral) (PA-PVB) taken from ref 21 is given for comparison.

on each carbon. On the left-hand side of Figure 3 we show the band structure in the energetically unfavorable situation with equally spaced carbons where no band gap between the π and π^* bands is found. Upon relaxation of the strained geometry a band gap of 1.6 eV opens up at Z in analogy to the Peierls distorted H chain. For a comprehensive discussion of the subject, we refer to the literature.[40] As the smallest energy difference of the valence and conducting bands is at Z, we expect the low-energy optical spectrum to be dominated by $\pi^* \leftarrow \pi$ transitions starting at this symmetry point. In Figure 4 we show the calculated spectrum with the **E** vector lying parallel to the chain (i.e. **E**∥**z**). It was obtained by working out the oscillator strengths at 50 equally spaced **k** points along the one-dimensional irreducible Brillouin zone and fitting Gaussian lobes with half-widths of 1000 cm^{-1} ($\approx$0.12 eV) at the obtained line spectrum. We have cut the low-energy tail of the spectrum at the gap threshold, as we do not have computational information in this energy region.

Recently, a new synthesis approach to PA has been introduced.[53] This synthetic route utilizes transition metal ions complexed with poly(vinylbutyral) (PVB) as the polymerization catalyst and yields highly stable blends of PA with PVB. The absorption spectrum of this material is shown in the inset of Figure 4 for comparison.[21] The agreement between calculation and measurement is good, even though the experimental absorption peak is shifted to somewhat higher energy and is broader. This problem could be addressed by adapting the half-
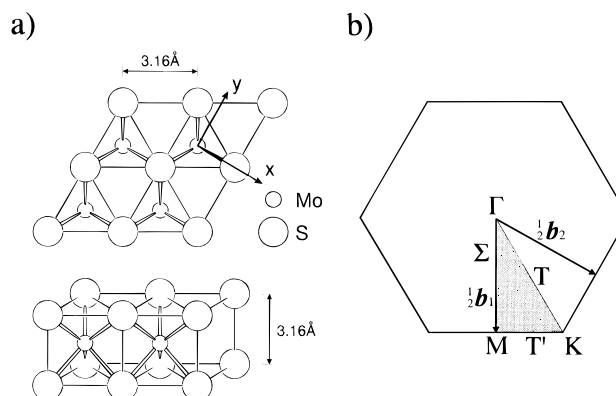

Figure 5. (a) MoS$_2$ layer structure with trigonal coordination of Mo. (b) Hexagonal Brillouin zone.

widths of the Gaussian lobes. It is, however, difficult to judge whether or not such a procedure is reasonable, as there are uncertainties in the measurement, too, like the effective conjugation lengths. Moreover, it should be noted that we have considered a single PA chain, thus neglecting the interaction between neighboring PA molecules. If we follow the development of the oscillator strengths of the $\pi^* \leftarrow \pi$ transition from the lowest to the highest energy (i.e. from Z to Γ) with values of 1.6 and 11.5 eV, respectively, we find the largest oscillator strength at Γ. This reflects the topological relationship of the PA π system with the Peierls distorted H chain and the linear $\cdots$A−B$\cdots$A−B$\cdots$A−B$\cdots$ system discussed above. The worked out spectrum given in Figure 4 is closely connected with the band encountered below 12 eV in Figure 2, where the absorption spectrum of the fictive A−B chain is depicted. On going from lower to higher absorption energy, i.e. from the edge to the center of the one-dimensional Brillouin zone, the oscillator strengths computed at distinct **k** points slowly increase (cf. also the dashed line in Figure 1b). Yet, we do not observe an absorption band that continuously increases in intensity with increasing absorption energy. The reason for this behavior can be clearly identified as due to the high density of states (DOS) found at the center and the edge of the Brillouin zone. Thus, the first prominent electronic absorption band in PA is indeed a $\pi^* \leftarrow \pi$ transition, and the characteristic shape is not governed by the transition matrix elements but by the high DOS encountered at the Z point (cf. eq 13).

MoS$_2$. The structure of $^2_\infty$[MoS$_2$] as already determined by Dickinson and Pauling in 1923 is shown in Figure 5a.[54] The distance between the two sulfur atoms within and across the chalcogenide plane is about 3.16 Å. Weak van-der-Waals-type stacking of such planes leads to two molybdenum sulfide polytypes, namely, 2H- and 3R-MoS$_2$. While the 2H modification gives rise to hexagonal crystals with an A, B, A, ... stacking sequence (space group D^4_{6h}), 3R-MoS$_2$ belongs to a rhombohedral Bravais lattice with an A, B, C, A, ... succession of the chalcogenide planes (space group C^5_{3v}). As interlayer interaction is weak, we may neglect it for the moment and focus on the description of the band structure and the absorption spectrum within a single MoS$_2$ layer that extends infinitely in two dimensions ($^2_\infty$[MoS$_2$]).

The band calculations were performed within the extended Hückel tight-binding method[39,55] modified as described in refs 10 and 38. The band structure along the hexagonal Brillouin zone (cf. Figure 5b) symmetry lines of a $^2_\infty$[MoS$_2$] layer along with the total DOS and the S(3s), S(3p), and Mo(4d) contributions are shown in Figure 6.[10] The top of the valence band is situated at Γ. From the DOS plot it is evident that the lowest band is mainly composed of S(3s) derived states. At the top of the valence band is the so-called d$_{z^2}$ band. It overlaps slightly
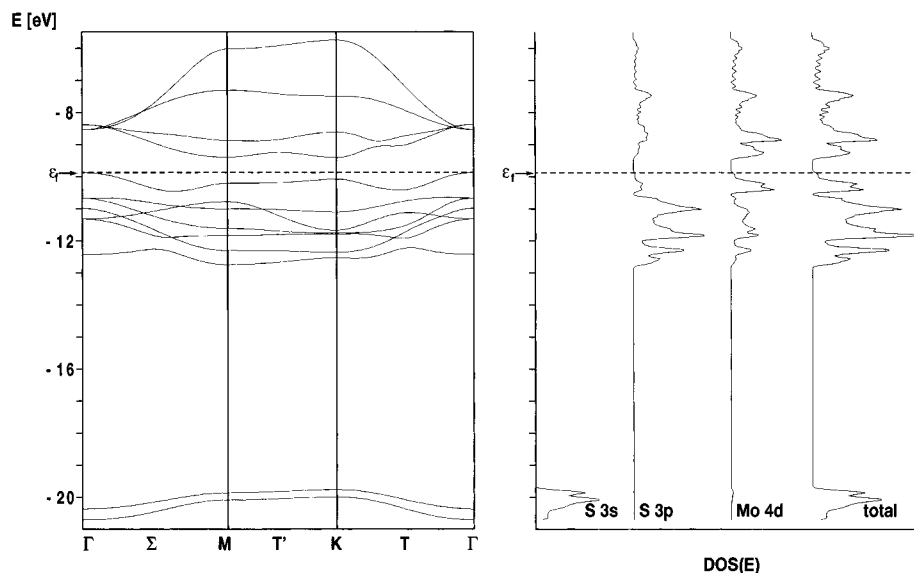
Figure 6. Band structure of the hexagonal Brillouin zone symmetry lines and density of states of a $^2_\infty[MoS_2]$ layer. The S(3s), S(3p), and Mo(4d) contributions to the DOS are projected out.
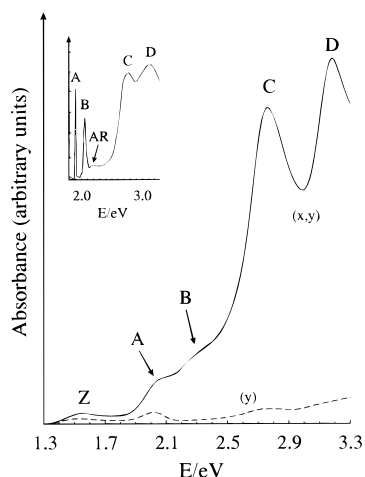

Figure 7. Calculated transmission spectrum with CEDiT in the energy range from 1.3 to 3.3 eV. Only transitions with **E** parallel to the slab are considered. Contributions from **y**-polarized absorptions are shown as a dashed line. For an easier comparison the energy axis is shifted by 0.59 eV to get exact agreement of the peaks C. In the inset the transmission spectrum of 3R-MoS$_2$ taken from ref 7 is given.

TABLE 3: Energies (in eV) of Prominent Features of the Spectra of the Two Polytypes of MoS$_2$ Compared with the EHTB−CEDiT Calculation; In the Last Column We Give the Averaged Difference of Experimental and Computed Absorption Bands

	2H-MoS$_2$	3R-MoS$_2$	EHTB−CEDiT	ΔE
Z			0.94	
A	1.910	1.908	1.44	0.47
B	2.112	2.057	1.68	0.40
C	2.760	2.758	2.17	0.59
D	3.175	3.126	2.58	0.57

A exciton in 2H-MoS$_2$. The bands C and D, respectively, are due to orbitally allowed interband absorptions.

The calculated spectrum (**E** ⊥ **z**) is given in Figure 7 along with the projected out **y**-polarized transitions (dashed line). To our knowledge no absorption spectrum with the **E** vector parallel to **z** (crystallographic *c* axis) has been reported. We will return to this point later. The spectrum was obtained by fitting Gaussian lobes with a half-width of 0.055 eV (450 cm^{-1}) to the computed line spectrum that resulted from considering all transitions from the seven valence bands to the four conduction bands (cf. Figure 6) at 190 **k** points in the IBZ of the hexagonal Bravais lattice. We have already mentioned that most band structure calculations, regardless of the method applied, underestimate the band gaps often by roughly half an electronvolt. For an easier comparison with experimental results we have thus shifted the energy axis by 0.59 eV to get exact agreement of the peaks C. Experimental and computed energies in electronvolts of the prominent spectral features are compared in Table 3.

By coincidence the coordinate system is set up such (cf. Figure 5a) that transition along **y**, even though not forbidden by symmetry, only carry low intensity; see dotted line in Figure 7. Symmetry arguments would equally predict transitions in **x** and **y**, as both axes (operators) remain the same upon reflection at a mirror plane running through the molybdenum centers. This requires the initial and final crystal orbitals to transform alike upon this symmetry operation. The two calculated peaks at 2.76 and 3.17 eV, respectively, may be readily identified as the absorptions at 2.76 and 3.175 eV reported in ref 7. The distance of the bands and their relative intensity are well produced. On the low-energy side of the spectrum we observe another peak (Z) at 1.53 eV which has not been reported so far. It is of low intensity and mainly of d−d character. Only the d_{z^2}, $d_{x^2-y^2}$, and d_{xy} orbitals, which transform evenly under the symmetry
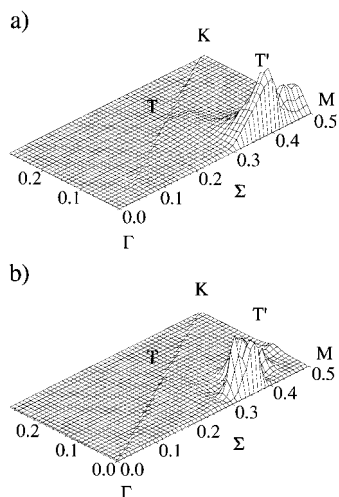
with the binding part of the valence band, which is predominantly of S(3p) character with mixed-in Mo(4d) contributions. The Fermi level is calculated to be at −9.87 eV. The smallest direct gap is situated at *K* and the smallest indirect gap goes from Γ to *K*, with values of 0.68 and 0.47 eV, respectively. These results are in good agreement with the experimental data and also with more sophisticated calculations.[56−58] The calculated band gaps are too small, however, which does not affect our conclusions; for more details see ref 10.

The transmission spectrum of MoS$_2$ with the light's **E** vector parallel to the slab was previously presented in 1969 by Wilson and Yoffe,[22] who introduced the labels A, B, C, D, ... to denote the absorption peaks in the direction of increasing photon energy. Later Beal et al. published better resolved transmission spectra measured at 5 K (cf. inset in Figure 7).[7,9] The two sharp absorption bands at 1.9 and 2.1 eV, respectively, were attributed to excitonic transitions on the grounds of different observations, like the strong temperature dependence of the line widths, the anti resonance "dip" AR observed at the high-energy side of peak B, and most of all, the presence of sharp fine structure corresponding to higher quantum number states (*n* = 2) for the

Electronic Transition Oscillator Strengths in Solids

J. Phys. Chem. B, Vol. 101, No. 29, 1997 **5673**

Figure 8. Oscillator strength plotted as a function of the respective **k** vector ($f_{fi}(\mathbf{k})$). The main line intensities are due to promotion of an electron from the CO immediately below the highest occupied crystal orbital (HOCO) to the lowest unoccupied crystal orbital (LUCO). (a) Contributions to the first excitonic transition A with **E** parallel to the slab in the energy range of ±0.12 eV about the main absorption (cf. Table 3). The strongest line absorption is found at $\mathbf{k}_A = (^{22}/_{57}, ^2/_{57})$ with an f_{fi} value of ~9.4 × 10⁻². (b) The same for exciton B with a maximum absorption at $\mathbf{k}_B = (^1/_3, ^2/_{57})$ and a corresponding f_{fi} of ~1.5.

Figure 9. Oscillator strength plotted as a function of the respective **k** vector. (a) Contributions to the first interband transition C with **E** parallel to the slab in the energy range of ±0.12 eV about the main absorption (cf. Table 3). (b) The same for the interband transition D.

operation described above, contribute to the oscillator strength. The small anisotropy of Z regarding the transitions in the **x** and **y** direction was to be expected. The two bands A and B, respectively, have already been attributed to orbitally allowed Mott−Wannier excitons by Wilson et al. It is therefore not surprising that we do not observe two sharp peaks in a model treating the electrons as delocalized throughout the solid. Two shoulders at 2.03 and 2.27 eV, respectively, can be identified instead.

Mott−Wannier excitons are formed by superimposing enough levels in a narrow region in **k** space near an orbitally allowed transition to form a well-localized wave packet.[1] In Figure 8a we have plotted the calculated oscillator strengths as a function of the **k** vector ($f_{fi}(\mathbf{k})$) in an energy range of ±0.12 eV about the main intensity found at 2.03 eV. In Figure 8b the same projection technique is applied for exciton B (2.27 ± 0.12 eV). Analogous drawings are compiled in Figure 9a,b for the interband transitions C and D, respectively. Such figures are illustrative, as they show the origin of the examined transitions in **k** space. We state that absorptions along lines or points of high symmetry can only partially explain the computed absorption intensities; the entire IBZ has to be considered. It is surprising that transitions near Γ that have been interpreted by Wilson[22] and later by Bromley[59] as responsible for the low-energy bands A and B, respectively, make only a minimum contribution to the interband absorption C. Hence, construction of band structures on the basis of optical data alone may lead to wrong results. Even though the shoulders arising in the computed spectrum are confined to a small region in **k** space, we do not want to give the impression that such drawings can explain the sharp peaks A and B, respectively. Such reasoning would be especially doubtful if we added that at higher energies (e.g. peak D) more and more transitions from different $\psi_{i\mathbf{k}}-\psi_{f\mathbf{k}}$ pairs begin to contribute to the respective absorption bands in the considered energy range of ±0.12 eV about the band maximum. The "density of transitions" for the interband absorptions C and D, respectively, is almost twice that of the peaks A and B. The more transitions contributing to an absorption band, the more likely it is that they are distributed over a large area of **k** space. A more involved study including symmetry analysis of the respective crystal orbitals and the
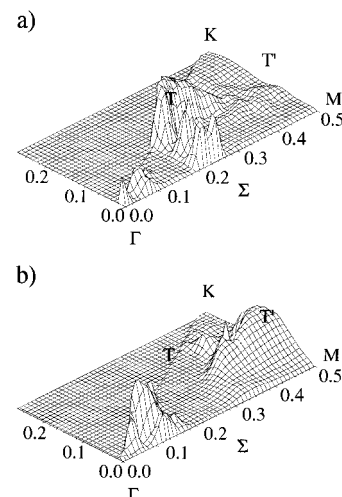
consideration of configuration interaction would be necessary. However, supported by the presence of an adjacent antiresonance "dip", labeled AR in the experimental spectrum and based on our computed data, we conclude that the excitons A and B can be understood in terms of a resonance phenomenon. The intensities hidden under the shoulders A and B of the computed spectrum are collected in the respective sharp absorption peaks. It is difficult to know about what **k** point we should start the construction of the localized excitonic states. However, we suggest the maximum line intensities found at about $\mathbf{k}_A = (^{22}/_{57}, ^2/_{57})$ and $\mathbf{k}_B = (^1/_3, ^2/_{57})$, respectively.

The transitions making the largest contribution to peaks A and B are of the charge-transfer type (Mo(d_{xy}) ← S($3p_y$)), exciton B exhibiting a greater covalent behavior. An electron is promoted from the CO located immediately below the highest occupied crystal orbital (HOCO) to the lowest unoccupied crystal orbital (LUCO). Roughly 30% of the intensity of the low-energy exciton is contributed by d−d transitions involving an electronic absorption from the HOCO to the superjacent LUCO in the considered region of **k** space. Both of these transitions are of the same symmetry and almost degenerate at the same **k** points. Whether this coincidental degeneracy enhances the exciton formation remains an open question. It seems probable, however, since we expect a condition of resonance to exist under this assumption.[60]

Beal et al. have discussed the difference in line width of the A exciton shown in the two MoS₂ polytypes. The line width in the 3R modification is about half of that found in the hexagonal 2H modification, where furthermore an $n = 2$ state in the Rydberg series is resolved.[7] On the other hand, electroabsorption studies[61] that measure binding energies directly from exciton and band edge signals have given similar values of the binding energy for the A exciton in 3R- and 2H-MoS₂. Beal et al. give an explanation for this apparent anomaly as due to layer−layer interaction and coupling of the electronic states in the direction of the **z** axis, which is stronger for the two-layer stacking sequence found in 2H-MoS₂ than for the rhombohedral three-layer stacking in the 3R configuration. Their finding is now supported by our calculation which predicts quite a large (Mo(d_{z^2})) contribution to exciton A. These orbitals are expected to interact stronger in the 2H modification. Moreover, it is known that the A and B splitting is sensitive to layer−layer interactions.[7,62]

In Figure 9a,b we give the $f_{fi}(\mathbf{k})$ plots for the absorption peaks C and D. Both of them have contributions from short **k** vectors

with maxima along the *T* line. Their intensities decrease rapidly as we move toward the Σ line. In contrast to the excitonic peaks A and B they have contributions from many interband transitions that are associated with the band crossings we observe in the conduction band region along the *T* line (cf. Figure 2). The main intensity of the interband absorptions C and D is, however, distributed over quite large regions in the irreducible Brillouin zone.

To our knowledge absorption spectra with **E**‖**z** have not been reported so far. They can, however, be calculated. One of our findings is that a relatively intense absorption band should arise between the mainly **x**-polarized C and D peaks and a much less intense one in the region of exciton B. Comparison of the calculated intensities is rather difficult, as the presented procedure requires full translational symmetry in the direction of the light vector, which is certainly not fulfilled in the $^{2}_{\infty}$[MoS$_2$] case. Or in other words, it is possible to compare the relative intensities of the transitions along the **z** axis, as we may compare the oscillator strengths of transitions along **x** and **y**. Comparison of **x** and **z** or **y** and **z** is, however, not possible, as the light wave certainly is affected by how many neighbor cells it hits while propagating throughout the solid.

4. Conclusions

We have presented a way to compute the oscillator strengths in extended structures within the EHTB method. Calculations on polyacetylene and the transition metal dichalcogenide MoS$_2$ have lead to promising results. The relative absorption energies and the corresponding intensities are well reproduced. Due to plotting of the oscillator strengths as a function of the **k** vector, we conclude for MoS$_2$ that a great deal of the absorption intensities is contributed by excitations at low-symmetry points within the IBZ. As we are given a computational tool to determine the nature of the electronic transitions by inspection of the crystal orbitals involved, it seems possible that the concept of charge transfer, d* ← d, π* ← π, and σ* ← σ transitions, that has proven successful in the description of excited states in molecules, can be extended to solids. We expect that this procedure may help to gain insight into the electronic absorption spectra of other extended structures.

References and Notes

(1) Ashcroft, N. W.; Mermin, N. D. *Solid State Physics*; Saunders College Publishing: Philadelphia, 1976.

(2) Drude, P. *Ann. Phys.* **1900**, *1*, 566.

(3) Drude, P. *Ann. Phys.* **1900**, *3*, 369.

(4) Hoffmann, R. *A Chemist's View of Bonding in Extended Structures*; Verlag Chemie: Weinheim, 1988.

(5) Magonov, S. N.; Whangbo, M.-H. *Adv. Mater.* **1994**, *6*, 355.

(6) Calzaferri, G.; Rytz, R. *J. Phys. Chem.* **1996**, *100*, 11122.

(7) Beal, A. R.; Knights, J. C.; Liang, W. Y. *J. Phys. C: Solid State Phys.* **1972**, *5*, 3540.

(8) Al-Hilli, A. A.; Evans, B. L. *J. Cryst. Growth* **1972**, *15*, 93.

(9) Beal, A. R.; Hughes, H. P. *J. Phys. C: Solid State Phys.* **1979**, *12*, 881.

(10) Brändle, M.; Calzaferri, G.; Lanz, M. *Chem. Phys.* **1995**, *201*, 141.

(11) Persans, P. D.; Lu, E.; Haus, J.; Wagoner, G.; Ruppert, A. F. *Mat. Res. Symp. Proc. Vol.* **1990**, *195*, 591.

(12) Würfel, P. *Physik der Solarzellen*; Spektrum Akademischer Verlag: Heidelberg, 1995.

(13) Wolfsberg, M.; Helmholz, L. *J. Chem. Phys.* **1952**, *20*, 837.

(14) Ballhausen, C. J.; Gray, H. B. *Molecular Orbital Theory*; W. A. Benjamin, Inc.: Amsterdam, 1965.

(15) Calzaferri, G.; Rytz, R. *J. Phys. Chem.* **1995**, *99* (32), 12141.

(16) Hansen, A. E. *Int. J. Quantum Chem.* **1971**, *S4*, 473.

(17) Hansen, A. E.; Bouman, T. D. *Mol. Phys.* **1979**, *37* (6), 1713.

(18) Chen, J. C. Y. *J. Chem. Phys.* **1964**, *40*, 615.

(19) Baker, J. D.; Zerner, M. C. *J. Phys. Chem.* **1991**, *95*, 8614.

(20) Yu, J.; Baker, J. D.; Zerner, M. C. *Int. J. Quantum Chem.: Chem. Symp.* **1992**, *26*, 475.

(21) Sariciftci, N. S.; Kobryanskii, V. M.; Reghu, M.; Smilowitu, L.; Halvorson, C.; Hagler, T. W.; Mihailovic, D.; Heeger, A. J. *Synth. Met.* **1993**, *53*, 161.

(22) Wilson, J. A.; Yoffe, A. D. Academic Press, Inc.: New York and London, 1969; Vol. 18, p 193.

(23) Mulliken, R. S. *J. Chem. Phys.* **1939**, *7*, 20.

(24) McGlynn, S. P.; Vanquickenborne, L. G.; Kinoshita, M.; Carroll, D. G. *Introduction to Applied Quantum Chemistry*; Hoft, Rinehart and Winston, Inc.: New York, 1972.

(25) Herzberg, G. *Molecular Spectra and Molecular Structure. I. Spectra of Diatomic Molecules*; Van Nostrand Reinhold: New York, 1950.

(26) Ramírez, R.; Böhm, M. C. *Int. J. Quantum Chem.* **1986**, *XXX*, 391.

(27) Bethe, H. A.; Salpeter, E. E. *Quantum Mechanics of One- and Two-Electron Atoms*; Cornell Univ. Press: Ithaca, NY, 1957.

(28) Atkins, P. W. *Molecular Quantum Mechanics*, 2nd ed.; Oxford University Press: Oxford and New York, 1983.

(29) Adams, E. N. *J. Chem. Phys.* **1953**, *21*, 2013.

(30) Blount, E. I. In *Solid State Physics—Advances in Research and Applications*, Vol. 13; Seitz, F., Turnbull, D., Eds.; Academic Press, Inc.: New York, and London, 1962.

(31) Genkin, V. M.; Mednis, P. M. *Zh. Eksp. Teor. Fiz*, **1968**, *54*, 1137.

(32) Cojan, C.; Agrawal, G. P.; Flytzanis, C. *Phys. Rev. B* **1977**, *15* (2), 909.

(33) Madelung, O. *Festkörpertheorie II*; Springer-Verlag: Heidelberg, Berlin, New York, 1972.

(34) Fuchs, K. *Proc. R. Soc. A* **1940**, *176*, 214.

(35) Lowe, J. P. *Quantum Chemistry*, 2nd ed.; Academic Press, Inc.: New York and London, 1993.

(36) Howell, J.; Rossi, A.; Wallace, D.; Haraki, K.; Hoffmann, R. *ICON8, Quantum Chemistry Program Performing Extended Hückel Calculation*; Quantum Chemical Program Exchange QCPE, 1978.

(37) Calzaferri, G.; Rytz, R.; Brändle, M. *ICON-EDiT, Extended Hückel Molecular Orbital and Transition Dipole Moment Calculations*; available via http://iacrs1.unibe.ch/(130.92.11.3), 1995.

(38) Brändle, M.; Calzaferri, G. *Helv. Chim. Acta* **1993**, *76*, 2350.

(39) Whangbo, M.-H.; Evain, M.; Hughbanks, T.; Kertesz, M.; Wijeysekera, S.; Wiler, C.; Zheng, C.; Hoffmann, R. *EHMACC Extended Hückel Molecular, Crystal and Properties Package*; Quantum Chemical Program Exchange QCPE, 1989.

(40) Hoffmann, R.; Janiak, C.; Kollmar, C. *Macromolecules* **1991**, *24* (13), 3725.

(41) Skotheim, T. A. *Handbook of Conducting Polymers*; Marcel Dekker: New York, 1986; Vols. I and II.

(42) Shirakawa, H.; Ikeda, S. *Polym. J.* **1971**, *2*, 231.

(43) Shirakawa, H.; Ikeda, S. *J. Polymer Sci., Chem.* **1974**, *12*, 929.

(44) Lennard-Jones, J. E. *Proc. R. Soc. A* **1937**, *158*, 280.

(45) Coulson, C. A. *Proc. R. Soc. A* **1938**, *164*, 383.

(46) Naarmann, H.; Theophilou, N. *Synth. Met.* **1987**, *22*, 1.

(47) Longuet-Higgins, H.; Salem, L. *Proc. R. Soc. A* **1959**, 172.

(48) Fincher, C. R., Jr.; Chen, C.-E.; Heeger, A. J.; MacDiarmid, A. G.; Hastings, J. B. *Phys. Rev. Lett.* **1982**, *48*, 100.

(49) Billingham, N. C.; Calvert, P. D. *Advances in Polymer Science, Conducting Polymers and Molecular Recognition*; Springer-Verlag: Heidelberg, 1989; Vol. I.

(50) Yannoni, C. S.; Clarke, T. C. *Phys. Rev. Lett.* **1983**, *51*, 1191.

(51) Karpfen, A.; Petkov, J. *Theor. Chim. Acta* **1979**, *53*, 65.

(52) Suhai, S. *Chem. Phys. Lett.* **1983**, *96*, 619.

(53) Kobryanskii, V. M.; Tereshko, E. A. *Synth. Met.* **1990**, *37*, 33.

(54) Dickinson, R. G.; Pauling, L. *J. Am. Chem. Soc.* **1923**, *45*, 1466.

(55) Whangbo, M.-H.; Hoffmann, R. *J. Am. Chem. Soc.* **1978**, *100*, 6093.

(56) Coehoorn, R.; Haas, C.; Dijkstra, J.; Flipse, C. J. F.; de Groot, R. A.; Wold, A. *Phys. Rev. B* **1987**, *35*, 6195.

(57) Shepherd, F. R.; Williams, P. M. *J. Phys. C: Solid State Phys.* **1974**, *7*, 4427.

(58) McMenamin, J. C.; Spicer, W. E. *Phys. Rev. Lett.* **1972**, *29*, 1501.

(59) Bromley, R. A.; Murray, R. B.; Yoffe, A. D. *J. Phys. C: Solid State Phys.* **1972**, *5*, 759.

(60) Knox, R. S. *Theory of Excitons*; Academic Press: New York, 1963.

(61) Bordas, J. Ph.D. Theses; Cambridge University, 1972.

(62) Neville, R. A.; Evans, B. L. *Phys. Status Solidi B* **1976**, *73*, 597.

(63) Zonneyville, M. C.; Hoffmann, R. *Surf. Sci.* **1988**, *199*, 320.

(64) Clementi, E.; Roetti, C. *At. Data Nucl. Data Tables* **1974**, *14*, 439.

(65) Brändle, M.; Calzaferri, G. *Helv. Chim. Acta* **1993**, *76*, 924.